Investigation of hydrodynamics in high solid anaerobic digestion by particle image velocimetry and computational fluid dynamics: Role of mixing on flow field and dead zone reduction

Yuying Hu, Xiaohuan Zheng, Shihao Zhang, Wenjie Ye, Jing Wu, Souhila Poncin, Huai-Zhi Li

▶ **To cite this version:**

Yuying Hu, Xiaohuan Zheng, Shihao Zhang, Wenjie Ye, Jing Wu, et al.. Investigation of hydrodynamics in high solid anaerobic digestion by particle image velocimetry and computational fluid dynamics: Role of mixing on flow field and dead zone reduction. Bioresource Technology, 2021, 319, pp.124130. 10.1016/j.biortech.2020.124130 . hal-02946460

HAL Id: hal-02946460
https://hal.science/hal-02946460v1

Submitted on 23 Sep 2022

HAL is a multi-disciplinary open access archive for the deposit and dissemination of scientific research documents, whether they are published or not. The documents may come from teaching and research institutions in France or abroad, or from public or private research centers.

L'archive ouverte pluridisciplinaire **HAL**, est destinée au dépôt et à la diffusion de documents scientifiques de niveau recherche, publiés ou non, émanant des établissements d'enseignement et de recherche français ou étrangers, des laboratoires publics ou privés.

Distributed under a Creative Commons Attribution - NonCommercial 4.0 International License

Version of Record: https://www.sciencedirect.com/science/article/pii/S0960852420314048
Manuscript_acaf1bc8260819b78e948e706feac05a

Investigation of hydrodynamics in high solid anaerobic digestion by particle image velocimetry and computational fluid dynamics: role of mixing on flow field and dead zone reduction

Yuying Hu[a,b,c], Xiaohuan Zheng[a], Shihao Zhang[a], Wenjie Ye[a], Jing Wu[b], Souhila Poncin[c], Huai Z. Li[c*]

[a]*School of Civil Engineering and Architecture, East China Jiao Tong University, Nanchang, 330013, China*

[b] *State Key Joint Laboratory of Environment Simulation and Pollution Control, School of Environment, Tsinghua University, Beijing, 100084, China*

[c] *Laboratory of Reactions and Process Engineering, Université de Lorraine, CNRS, 1, rue Grandville, BP 20451, 54001 Nancy cedex, France*

[*]corresponding authors: Huai Z. Li
E-mail address: Huai-Zhi.Li@univ-lorraine.fr (H.Z. Li).

© 2020 published by Elsevier. This manuscript is made available under the CC BY NC user license
https://creativecommons.org/licenses/by-nc/4.0/

Abstract:

High solid anaerobic digestion (HSAD) was a potential organic waste treatment. Compared with low solid anaerobic digestion, it had the advantages of small footprint, less digestate, and low heating energy. However, HSAD's methane production is poor, mainly due to the complex hydrodynamics. In this study, computational fluid dynamics were utilized for HSAD's hydrodynamics investigation at 14.3% solid content and compared to the particle image velocimetry measurement. Then, effects of mixing on hydrodynamics were investigated. The results indicated that the diameter of impeller was critical for the radial mixing, and the distance between the impellers dictated the axial mixing. Besides, rotating speed affected flow velocities significantly, but displayed less effect on expanding the mixing range. Furthermore, HSAD's treating capacity could be increased at large extent by optimizing mixing. The visualization of the hydrodynamics in this study could potentially offer conceptual basis for HSAD's design in practical engineering.
Keywords: High solid anaerobic digestion, dead zone, hydrodynamic condition, computational fluid dynamics, particle image velocimetry.

1. Introduction

Anaerobic digestion could not only treat organic wastes but also recycle biogas [1, 2]. Compared with other organic waste treatment technology (e.g. incineration and sanitary landfill), anaerobic digestion is more favorable from the environmental aspect which meets the demand for sustainable development[3]. High solid anaerobic digestion (HSAD), which is conducted at solid content higher than 10%, attracts extensive attention recently [1, 2, 4, 5]. It has the advantages of small footprint, less digestate, and low heating energy [6]. Decidedly, HSAD is the mainstream of anaerobic digestion in a near future [2, 4, 5].

However, the flow pattern in HSAD is quite non-uniform and non-ideal [7]. HSAD's digestate is acknowledged as a highly viscous non-Newtonian fluid [8, 9] with the characteristics of shear-thinning, thixotropy and yield properties [7]. Incomplete mixing, short circuiting and the increment of inactive and stagnant zones usually occurred in HSAD system. These lead to the poor methane production and VS reduction of HSAD for the following reasons: (1) the poor hydrodynamics caused the accumulation of inhibition substrate like ammonia and volatile fatty acids (VFAs), which further lead to the ammonia or VFAs inhibition; (2) the inefficient mass and heat transfer also suppresses HSAD's performance[2, 10]. In this way, the better understanding of the complex hydraulics condition is crucial for HSAD's sufficient and stable operation. However, the relative reported investigation is still limited in this field.

Computational fluid dynamics (CFD) is a powerful tool which could be used for

the investigation of the flow pattern and mixing behavior in anaerobic digestion [11]. For example, CFD was used for the evaluation of flow field, turbulence intensity and mixing time in anaerobic co-digestion of chicken manure and food waste at 7% solid content [12]. Besides, the mixing quality in full scale biogas-mixed anaerobic digestion at 2.5% solid content was evaluated *via* CFD [11]. Azargoshasb [13] investigated the three phase hydrodynamics with the Eulerian multiphase approach and k -ε turbulence model (RNG) in a continuous stirred bioreactor. However, the work undertaken so far was usually focused on low solid anaerobic digestion with a solid content lower than 10%. The application of CFD in HSAD is still quite limited for the major reason that the flow field of HSAD is difficultly measurable due to the lack of efficient measuring methods, and thus the CFD simulation is not able to be validated.

It is commonly recognized that the Particle Image Velocimetry (PIV) technique is an efficient tool for quantifying transparent flow fields. It could not only display the velocity distribution but also provide the quantitative information of the full flow field. The application of PIV in AD flow field has attracted increasing attention recently. Jiang et al. [14] has adopted the classical Metzner–Otto method for the mean shear rate, and PIV was used for the visualization of the instantaneous velocity field in the reactor at ss of 37 g SS/L. The unconfined gas mixing in anaerobic digestion was estimated by PIV in Dapelo's study [15]. The present study mainly focused on the anaerobic digestion at low solid content. Such an application on HSAD was still rare to our best knowledge.

In our previous studies, novel insight was put towards the characteristics of HSAD's flow fields *via* PIV [7]. It was noted that transparent 3.00% wet laponite suspension was introduced as the working model fluids for the similarity in both the rheological and structural characteristics. Though flow field visualization *via* PIV could help understand HSAD's hydraulic condition, its application could only be conducted at lab scale. Thus, its guidance to practical engineering was not significant yet.

To conclude, the visualization of HSAD's flow field *via* PIV is essentially limited at the lab-scale, and CFD lacks the validation methods. In this study, HSAD's hydrodynamics was simulated by CFD and a comparison was performed with the PIV measuring results. The main advantages were as following: (1) the results were quite reliable because CFD results has been confirmed with the PIV measurements; (2) once validated at laboratory scale, the CFD approach could be applied to HSAD at different scales, including industrial size in practical applications. Besides, our previous finding revealed that the fluid around the impeller was mixed when only a single impeller was applied [7]. In this study, effects of both the impeller type and mixing speed on HSAD's flow fields and dead zone are quantitatively evaluated. This study offers a potential access to the complex hydrodynamics in HSAD at practical engineering scale *via* CFD and PIV, and was essential for the stable and efficient performance of HSAD.

2. Materials and methods

2.1 Characteristics of HSAD digesate

In this study, HSAD digestate was taken from an HSAD reactor treating swine manure at lab-scale. Its total solid content was 14.3% and the volatile solid content was 11.3%. It was widely accepted that HSAD digestate was considered as non-Newtonian fluid at high solid content [11, 16]. The rheological characteristics of HSAD digestate was determined by a rheometer (AR-G2, TA, USA) in the shear rate of 0-10 s^{-1}, and could be described as the power-law model [17]:

$$\eta = K\dot{\gamma}^{n-1}$$

where η referred to the non-Newtonian fluid viscosity, Pa·s; K the consistency index, Pa·s^n; $\dot{\gamma}$ the shear rate, s^{-1} and n the flow index. K and n were measured to be 52.8 Pa·s^n and 0.09 respectively.

2.2 Impeller pattern

In our previous study, only the fluid around the impeller could be mixed when HSAD was rotated with impeller of single stage[7]. Thus, in this study, different impeller diameter, impeller stages and the impeller types were taken into consideration to reveal their effects on flow field and dead zone distribution. The impellers were named as impeller A, impeller B and impeller C respectively. Besides, the mixing with impeller A, impeller B and impeller C were named as Case A, Case B and Case C respectively. The detailed description of the three impellers were as following:

(1) Impeller A was an impeller of double stages arranged abreast with the diameter of 50 mm. The distance between the two impellers was 50mm, and the impeller height was 10 mm. It was comparable to our previous study [7] to reveal the effects of impeller's stages on axial flow.

(2) Impeller B was designed as impeller of three stages with the diameter of 90 mm, and was investigated for revealing impeller diameter's effects on flow pattern. The distance between the two impellers was 40 mm, and the impeller height was 10 mm. Besides, the effects of the distance between the impeller's stages on HSAD's flow field could also be evaluated.

(3) Impeller C was a ribbon impeller with the diameter of 90 mm. The impeller height was 140 mm. The relative study was used to reveal the effect of the impeller's type on the fluidity pattern.

2.3 CFD simulation

In this study, CFD simulation was performed *via* a commercial CFD software, ANSYS FLUENT 18.0. Considering that the HSAD digestate was non-Newtonian fluid of high viscosity and poor fluidity, the effect of produced biogas was limited on HSAD's hydrodynamics [12, 18-20]. In this way, the interaction between biogas and HSAD digestate was voluntarily neglected as suggested in the previous studies [12, 18-20]. The geometry and mesh of both the reactor and impellers were generated using GAMBIT 2.4.6. The number of Case A, B and C grids were 312,696, 447,058, 731,636 respectively. The minimum and maximum cell volume of each case were shown in Table 1. Afterwards, the obtained simulated results were compared with the PIV measured results to see whether they are reliable.

The flow and mixing facility could be assessed by the possible dead zone[9], in which the velocity magnitude is below 0.001m/s[21]. Dead zone was considered stagnant and few mass transfer was taken place. In this way, the anaerobic digestion could be considered inefficient in such zone. In other words, the dead zone occupying reactor volume and consuming input energy contributes uselessly to the whole reaction and reactor's efficiency.

2.4 Comparison with PIV measurements

2.4.1 Selection of the model fluid

PIV could only be employed for the flow field measurements in transparent fluids, but sometimes the targeted fluid was opaque. Thus, the transparent model fluid was usually used to mimic real opaque fluids like blood[22], cementitious composites[23] and so on. In our previous study, 3.00% (wt) laponite suspension was selected as the model fluid for their similarity in both rheological and structural properties compared to HSAD [7]. The rheological properties were measured by a rheometer (AR-G2, TA, USA) in the shear rate of 1 - 10 s^{-1}. Besides, 3.00% (wt) laponite suspension was a structural colloid-liquid suspension, which is similar to the HSAD digestate. In this way, 3.00% (wt) laponite was chosen as the model fluid. The visualization of HSAD was only conducted at 14.3%.

2.4.2 PIV measurement

The detailed description of the experimental PIV technique could be found in our previous study[7], and was summarized as follows. A transparent cylinder reactor which was continuously stirring with impeller A was filled with the model fluid (3.00% (wt) laponite suspension). The diameter and the height of the reactor was 100 mm and 200 mm respectively. The height of the working fluid was 120 mm. In order to avoid the optical deformation due to the cylinder curvature, the reactor was placed in a transparent square vessel filled up with water whose refractive index (1.33) was the

same with that of 3.00% (wt) laponite suspension (1.33 [22]).

Afterwards, PIV measurements were conducted. The PIV instrument (Dantec Dynamics, Denmark) used in this study mainly composed of: a Dual Power 30-15 Laser, a numerical CMOS camera, a central control unity and a computer.

The results of flow fields were computed through DynamicStudio software (Dantec Dynamics, Denmark). The produced flow fields were compared with the CFD simulation results to see whether they were reliable. If the CFD simulation was justified, the simulation was proved to be feasible and possibly extrapolated to installations of higher scale.

2.5 Computations

Generalized Reynolds number for non-Newtonian fluids was utilized for the characterization the flow pattern according to previous study[7, 23]:

$$Re = \frac{\rho N^{2-n} D^2}{K} \quad (1)$$

where Re is the generalized Reynolds number, ρ is the density of the fluid, kg·m^{-3}, N is the rotation speed, s^{-1}, D is the diameter of the impeller, m and K is the consistency, Pa·s^n; n is the flow index.

3. Results and Discussion

3.1 Comparison of CFD simulation with PIV measurement

In this study, our target was the investigation of HSAD's flow fields. PIV could only be employed for the flow field measurements in transparent fluids, but HSAD's digestate was opaque indeed. Thus, a model fluid, whose rheological and structural properties were similar to those of HSAD digestate, was utilized for PIV measurements to mimic HSAD's flow fields. As for the CFD approach, it was a numerical simulation technique which computed the flow fields based on the rheological properties of HSAD's digestate. In summary, the visualization of HSAD's flow field by PIV measurement in a model fluid could assess the reliability of CFD simulation before the extrapolation of CFD in real reactors involving other scales

The comparison of CFD simulation and PIV measurement (as mentioned in Section 2.4) was conducted in Case A at 100 rpm. The result of the CFD simulation was quite similar to that of PIV. Both of them revealed that the mixing region was only effective around the impeller, and the flow velocities around the impeller was around 0.1 m/s. However, there existed a difference that the flow field around the impeller measured by PIV was quite irregular compared with that of CFD modeling. This was closely related to the fact that PIV measurements were conducted with a model fluid and there existed some experimental fluctuations and noise, but CFD

simulation was an idealized numerical approach. To conclude, the CFD simulation was considered to be reliable. The visualization could potentially provide useful insight into the critical hydrodynamics for the practical engineering.

3.2 Role of mixing

3.2.1 Visualization of Case A's hydrodynamics

Flow fields in case A at different rotating speeds were graphically described in Fig. 1a. Obviously, the mixing region was just around the impeller at the low rotating speed of 50 rpm, 100 rpm, 150 rpm and 200 rpm. This phenomenon was quite similar to the experimental results measured by PIV in our previous study when only impeller of a single stage was used for mixing [7].

As the rotating speed continued to increase, it could be observed that the flow between the two impellers was strengthened gradually. In other words, compared with HSAD's flow field mixed with the impeller of a single stage observed in our previous study, increasing the number of impeller's stages was helpful to the mixing in the region between the impellers at high rotating speeds. Besides, it is worth noting that the flow near the axis was stagnant even at the rotating speed of 300 rpm. Furthermore, the highest flow velocities occurred at the tip of the impeller, and was closely related to the fact that the tip speed was highest. Flow velocities was getting lower gradually from the tip due to the existence of HASD digestate's high viscosity.

Rotating speed could increase both the flow velocities and mixing range, but its efficiency on expanding HSAD's mixing range was limited. For example, sufficient mixing was achieved in the range of x = -25mm – 25mm, y = 10 mm – 30 mm, 60 mm – 80mm at rotating speed of 50 rpm, and it increased to x = -40mm – 40mm, y = 0 mm – 90mm when the rotating speed was increased to 300 rpm. Furthermore, the region (y = 90 mm –150 mm) could be difficultly mixed even at the rotating speed of 300 rpm. In summarizing, both the radial and axial mixing was strengthened by increasing the rotating speed, however with a limited efficiency.

The spatial distribution of radial velocity at x = 20 mm was investigated. It could be observed that in the position near the impeller, the fluid was mixed vigorously with high velocities. The closer to the impeller the velocity was higher. Besides, the radial velocity at x = 20 mm increased with the rotating speed. Furthermore, it was interesting to note that the region between the impeller's stages was quiescent at low rotating speed (50 rpm), but became sufficiently mixed at high rotating speeds, e.g. rotating speed higher than 200 rpm. Furthermore, the region $y > 90$ mm was not mixed at all, even at the rotating speed of 300 rpm (Re = 2550).

The axial velocity was evaluated at y = 20 mm and 70 mm, referred to the central plane of the two impellers respectively. The axial velocity at these two planes was quite similar to each other, indicating that the mixing around the two stages was quite dependent in this case. Furthermore, the axial flow region expanded with the rotating speed. It was 5 mm – 31mm, 5 mm – 38mm, 5 mm – 42mm, 5 mm – 47mm at 50, 100, 150, 200, 250,300 rpm respectively. Logically, the flow velocity increased with

the rotating speed too.

3.2.2 Visualization of Case B's hydrodynamics

The flow field in the HSAD reactor mixed by the impeller B was illustrated in Fig. 1b. Compared to Case A, Case B presented flow field with higher velocities at each corresponding rotating speed. This was closely related to the fact that the more impellers consumed more power at the same rotating speed. Thus, faster mixing was achieved in case B. Obviously, the mixing area was around the different stages of the impellers independently, and the mixing between the stages was not significantly enough at the rotating speed of 50 rpm. However, as the rotating speed further increased, the area between three stages was mixed gradually. This was quite different from the findings in case A where the area between the stages was only mixed at the rotating speed ＞ 200 rpm. These phenomena closely related to the distance between the two stages, i.e. the stages were closer and the area between them was easier to be mixed. In addition, both the flow velocities and mixing area were increased with the rotating speed. The radial mixing was achieved at each rotating speed, this proved again that the radial mixing was mainly determined by the diameter of the impeller at large extent rather than the rotating speed in such complex fluids, which corresponded to the observation in case A. Furthermore, the axial mixing was achieved in the range of y = 20 mm – 140 mm at rotating speed of 50 rpm, and extended to 10 mm –150 mm as the rotating speed increased to 300 rpm. Compared to the axial mixing in Case A (the range of y = 10 mm – 90 mm), the axial mixing of y = 20 mm – 140 mm in Case B seemed to confirm the role played by the stages of impeller. On the other side, similar to case A, flow velocities were highest at the tip of each impeller, and was gradually decreased to surrounding because of the high viscosity.

The radial velocities at x = 20 mm were investigated. It could be observed that the radial velocities between the stages were about 0.02 m/s at 50 rpm. This was quite different from that in case A where the radial velocities between the stages were close to 0 m/s at 50 rpm. The difference between the two cases could arise from the distance between stages of the impellers: closer distance, easier flow driven. Furthermore, both the flow region and flow velocities increased with the rotating speed. On the other side, there were also some findings similar to Case A: the velocities near the impeller were higher and the radial velocities increased as the rotating speed increased.

The axial velocities at y = 40, 80, 120 mm, referred to the central plane of the three impellers, were investigated. Unambiguously, the axial mixing around the three stages of the impeller was quite similar to each other. The axial mixing region was sufficient in this case, and depended on the diameter of the impeller. In addition, the axial velocities also increased with the rotating speed.

3.2.3 Visualization of Case C's hydrodynamics

The flow field in the HSAD induced by a ribbon impeller at different rotating speeds was presented in Fig.1c. It could be observed that the mixing was quite effective in the edge of the reactor, and then centralized gradually with the increasing rotating speed. This behavior was quite different from those in case A and case B

where the mixing was more efficient in the central part of the reactor than the edge. The radial mixing was achieved at x = -50 mm – -30 mm and x = 30 mm – 50 mm at the rotating speed of 50 rpm, but increased to x = -50 mm – 50 mm at the rotating speed of 300 rpm. The flow velocities increased with the rotating speed. Furthermore, the axial mixing was efficient even at the low rotating speed. It could be concluded that the ribbon impeller was more suitable for achieving the efficient mixing in HSAD compared to other impellers investigated here.

Furthermore, the spatial distribution of axial and radial velocities were quite complex. However, both axial and radial mixing was quite efficient in the whole reactor. For this reason, the ribbon impeller could achieve an efficient mixing even at low rotating speeds.

3.3 Dead zone reduction

The spatial distribution of dead zone in Case A could be found in Fig. 2a. The dead zone decreased with the rotating speed. It is worth noting that the region between the two stages of the impeller was a dead zone at the very beginning when the rotating speed was 50 rpm. However, the flow in this region was strengthened gradually as the rotating speed was increased, and the mixing in this zone became efficient at 300 rpm. Furthermore, it was worth noting that the zone in the upper section of the working fluid was dead zone even at the rotating speed of 300 rpm.

The ratio of the dead zone at different rotating speeds in Case A was shown in Fig. 2b. It could be observed that dead zone comprised for quite large fraction in the HSAD reactor, and ranged between 65.2% – 90.5%. That is to say the efficient flow and mixing was only achieved in 9.5% – 34.8% active volume of the whole reactor. This indicated that the potential in increasing the treating capacity of HSAD was huge. In this regard, the inefficient mixing could be one of the major explanations for HSAD's poor methane production. Besides, increasing rotating speed of the impeller could decrease the ratio of dead zone to some extent, but the decrement was not sufficient. The dead zone ratio was in reverse linear relationship with rotating speed (50 – 300 rpm) with the R^2 of 0.9871, and could be described as follows:

$$y = -0.1x + 94.067 \quad (1)$$

where x was the rotating speed (rpm), and y was the volume ratio of dead zone (%).

As for the case B, the dead zone was quite limited in the reactor (Fig.2 a), i.e. dead zone only occupied in the edge and bottom of the reactor. It is worth noting that the zone between each impeller was active even at 50 rpm. In conclude, effective axial mixing could be achieved when the distance between the stages of impellers was close, and the radial mixing could be achieved when the diameter of the impeller is large enough.

The relationship between the dead zone and rotating speed in Case B was shown in Fig.2b. Compared to Case A, the dead zone ratio of case B was much lower (7.1% - 18.4%). This was closely related the fact that the more impellers consumed logically more power at the same rotating speed. The effect of the rotating speed on the reduction of the dead zone in case B was much less obvious. Only 11.3% dead zone

was reduced when the rotating speed was increased from 50 to 300 rpm. This indicated that increasing rotating speed was not necessary for decreasing the dead zone ratio in HSAD.

The distribution of dead zone in Case C was presented in Fig.2a. At 50rpm, the dead zone in Case C was quite limited, only occupying the edge of the reactor. As the rotating speed continuing increased, the dead zone disappeared gradually.

The ratio of dead zone was quite small, typically around 4.4% – 5.9% when the rotating speed was 50 – 300 rpm. This indicated that the ribbon impeller could achieve efficient mixing even at 50 rpm. Furthermore, the increasing of rotating speed seemed to induce negligible effect on the reduction of the dead zone which was relatively stable at 50 – 300 rpm. Thus, the ribbon impeller could be considered suitable for HSAD's mixing.

The following observations can be drawn by comparing the mixing efficiency in each case:

(1) The mixing in Case A seemed to be poorest. The ratio of the dead zone could be as high as 90.5%, increasing rotating speed could strengthen the flow and mixing to some extent.

(2) The flow and mixing in Case B were more effective than Case A. The ratio of the dead zone ranged from 7.1% to 18.4%. The rotating speed played a negligible role in its reduction.

(3) In Case C, the mixing was quite efficient. The dead zone ratio was only 4.4% - 5.9%. The rotating speed almost had no effect on the dead zone.

Among these three types of the impellers, the ribbon impeller was the most suitable for the HSAD mixing at any rotating speed (50 rpm – 300 rpm). However, the energy consumption of the ribbon impeller was too high to be applied in the practical engineering. In this way, multiple impellers arranged abreast was recommended for the HSAD. In particular, special attention should be paid to the impeller's diameter and the distance between stages.

3.4 Practical implication and perspectives

From the above-mentioned observations, it was beyond our expectation that the HSAD's dead zone ratio in each case displayed significant difference: the efficient active volume (total volume – dead zone) in Case A, Case B and Case C were 9.5 % – 34.8%, 81.6% – 92.9% and 94.1% – 95.6% respectively. The proper selection of the mixing equipment could increase the treating capacity at large extent. Without any doubt, such a potential increment in treating capacity confirms the attraction of HSAD at large extent. In this way, the present study throws new insight to the flow pattern in an efficient AD system, especially at high solid content. It could also provide some fundamental information for the design and optimization of HSAD reactor.

In the future, the mixing consumption should also be evaluated. Proper mixing should be selected based on the power consumption, flow pattern and reactor performance. Besides, the effect of scale-up on the flow field of HSAD should also be quantified, for the reason that there existed some difference between the flow field in

the industrial and lab-scale HSAD systems.

4. Conclusion

The visualization of HSAD's flow fields was numerically simulated by the CFD approach, then compared with the experimental PIV results. The validated CFD approach could then be extended to real reactors involving different scales. Besides, the radial mixing of HSAD depended mainly on impeller's diameter, as well as the distance between stages. The effect of the rotating speed was significant on flow velocities, and contrariwise relatively limited on mixing range. The proper selection of the mixing equipment could possibly increase both the treating capacity and methane production. This could reinforce assuredly the attraction of HSAD in industrial applications.

Acknowledgments:

Financial support for this research was provided by the Natural Science Foundation of China (51908214), Primary Research & Development Plan of Jiangxi (20192BBH80009, 20202BAB213020), Science and technology research project of Jiangxi Provincial Department of Education (GJJ180298) and National Students' platform for innovation and entrepreneurship training program (201910404011). Supplementary data associated with this article can be found, in the online version.

Notes:

All authors declare no actual or potential conflict of interest.

Reference

[1] Y.Y. Hu, J. Wu, H.Z. Li, S. Poncin, K.J. Wang, J.E. Zuo. Study of an enhanced dry anaerobic digestion of swine manure: Performance and microbial community property[J]. Bioresource Technology, 2019,282:353-360.

[2] W. Peng, F. Lü, L. Hao, H. Zhang, L. Shao, P. He. Digestate management for high-solid anaerobic digestion of organic wastes: A review[J]. Bioresource Technology, 2020,297:122485.

[3] X. Li, S. Chen, B. Dong, X. Dai. New insight into the effect of thermal hydrolysis on high solid sludge anaerobic digestion: Conversion pathway of volatile sulphur compounds[J]. Chemosphere, 2020,244:125466.

[4] Y. Fan, Z. Lei, X. Yang, M. Kobayashi, Y. Adachi, Z. Zhang, K. Shimizu. Effect of nano-bubble water on high solid anaerobic digestion of pig manure: Focus on digestion stability, methanogenesis performance and related mechanisms[J]. Bioresource Technology, 2020,315:123793.

[5] H. Nam Joey Ting, L. Lin, R. Bello Cruz, B. Chowdhury, I. Karidio, H. Zaman, B. Ranjan Dhar. Transitions of microbial communities in the solid and liquid phases during high-solids anaerobic digestion of organic fraction of municipal solid waste[J]. Bioresource Technology, 2020:123951.

[6] H.-G. Guo, Q.-L. Chen, H.-W. Hu, J.-Z. He. High-solid anaerobic co-digestion of pig manure with lignite promotes methane production[J]. Journal of Cleaner Production, 2020,258:120695.
[7] Y. Hu, J. Wu, S. Poncin, Z. Cao, Z. Li, H.Z. Li. Flow field investigation of high solid anaerobic digestion by Particle Image Velocimetry (PIV)[J]. Science of The Total Environment, 2018,626:592-602.
[8] L. Yu, J. Ma, S. Chen. Numerical simulation of mechanical mixing in high solid anaerobic digester[J]. Bioresource Technology, 2011,102(2):1012-1018.
[9] G. Leonzio. Study of mixing systems and geometric configurations for anaerobic digesters using CFD analysis[J]. Renewable Energy, 2018,123 578-589.
[10] Y.-y. Hu, C. Pan, X. Zheng, F. Hu, L. Xu, G. Xu, Y. Jian, X. Peng. Prediction and optimization of adsorption properties for Cs+on NiSiO@NiAlFe LDHs hollow spheres from aqueous solution: Kinetics, isotherms, and BBD model[J]. Journal of Hazardous Materials, 2020:123374.
[11] D. Dapelo, J. Bridgeman. Assessment of mixing quality in full-scale, biogas-mixed anaerobic digestion using CFD[J]. Bioresource Technology, 2018,265:480-489.
[12] L. Mao, J. Zhang, Y. Dai, Y.-W. Tong. Effects of mixing time on methane production from anaerobic co-digestion of food waste and chicken manure: Experimental studies and CFD analysis[J]. Bioresource Technology, 2019,294:122177.
[13] S.M.M. H. Azargoshasb , T. Amani b, A. Jafari c, M. Nosrati Three-phase CFD simulation coupled with population balance equations of anaerobic syntrophic acidogenesis and methanogenesis reactions in a continuous stirred bioreactor[J]. Journal of Industrial and Engineering Chemistry, 2015,27:207–217.
[14] J. Jiang, J. Wu, S. Poncin, H.Z. Li. Effect of hydrodynamic shear on biogas production and granule characteristics in a continuous stirred tank reactor[J]. Process Biochemistry, 2016,51(3):345-351.
[15] D. Dapelo, R. Trunk, M.J. Krause, J. Bridgeman. Towards Lattice-Boltzmann modelling of unconfined gas mixing in anaerobic digestion[J]. Computers & Fluids, 2019,180:11-21.
[16] J. Jiang, J. Wu, S. Poncin, H.Z. Li. Rheological characterization of digested sludge by solid sphere impact[J]. Bioresource Technology, 2016,218:301-306.
[17] M. Meister, M. Rezavand, C. Ebner, T. Pümpel, W. Rauch. Mixing non-Newtonian flows in anaerobic digesters by impellers and pumped recirculation[J]. Advances in Engineering Software, 2018,115:194-203.
[18] Y. Zhang, G. Yu, L. Yu, M.A.H. Siddhu, M. Gao, A.A. Abdeltawab, S.S. Al-Deyab, X. Chen. Computational fluid dynamics study on mixing mode and power consumption in anaerobic mono- and co-digestion[J]. Bioresource Technology, 2016,203:166-172.
[19] J. Zhang, Q. Qi, L. Mao, Y. He, K.-C. Loh, Y. Wah Tong. Mixing strategies – Activated carbon nexus: Rapid start-up of thermophilic anaerobic digestion with the mesophilic anaerobic sludge as inoculum[J]. Bioresource Technology, 2020,310:123401.
[20] X. Zhai, I.D. Kariyama, B. Wu. Investigation of the effect of intermittent minimal mixing intensity on methane production during anaerobic digestion of dairy manure[J]. Computers and Electronics in Agriculture, 2018,155:121-129.
[21] B. Wu, S. Chen. CFD simulation of non-Newtonian fluid flow in anaerobic digesters[J]. 2008,99(3):700-711.
[22] Y.M. Nimdeo, Y.M. Joshi, K. Muralidhar. Refractive index measurement of sol forming Laponite JS dispersion using interferometry[J]. Applied Clay Science, 2016,123:272-278.
[23] N.M. Entsar. Mixing process of apple juice concentrate[J]. Int. J. Nutr. Food Sci, 2016(5):1-6.

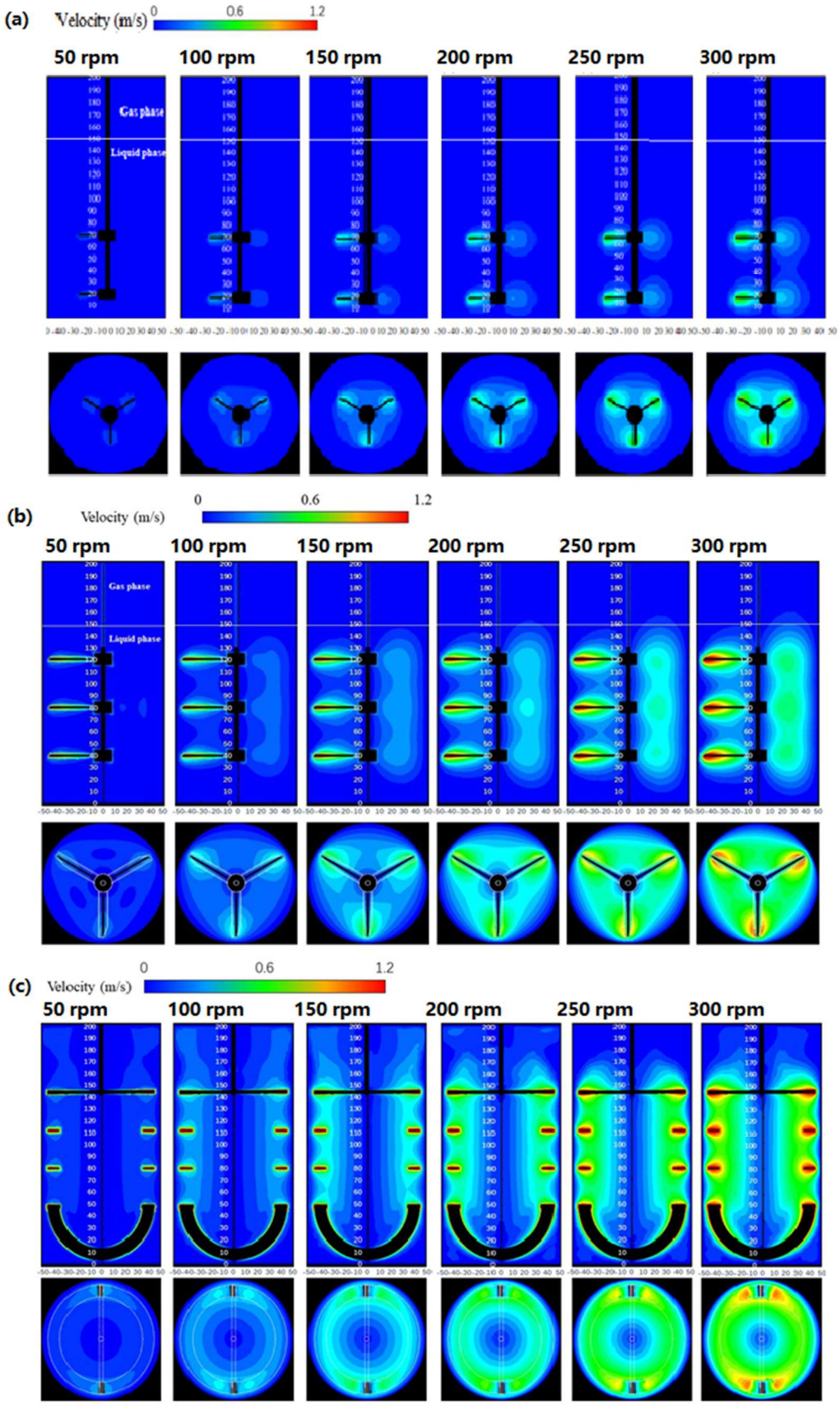

Fig. 1 Flow field at various rotating speeds of (a) Case A, (b) Case B and (c) Case C

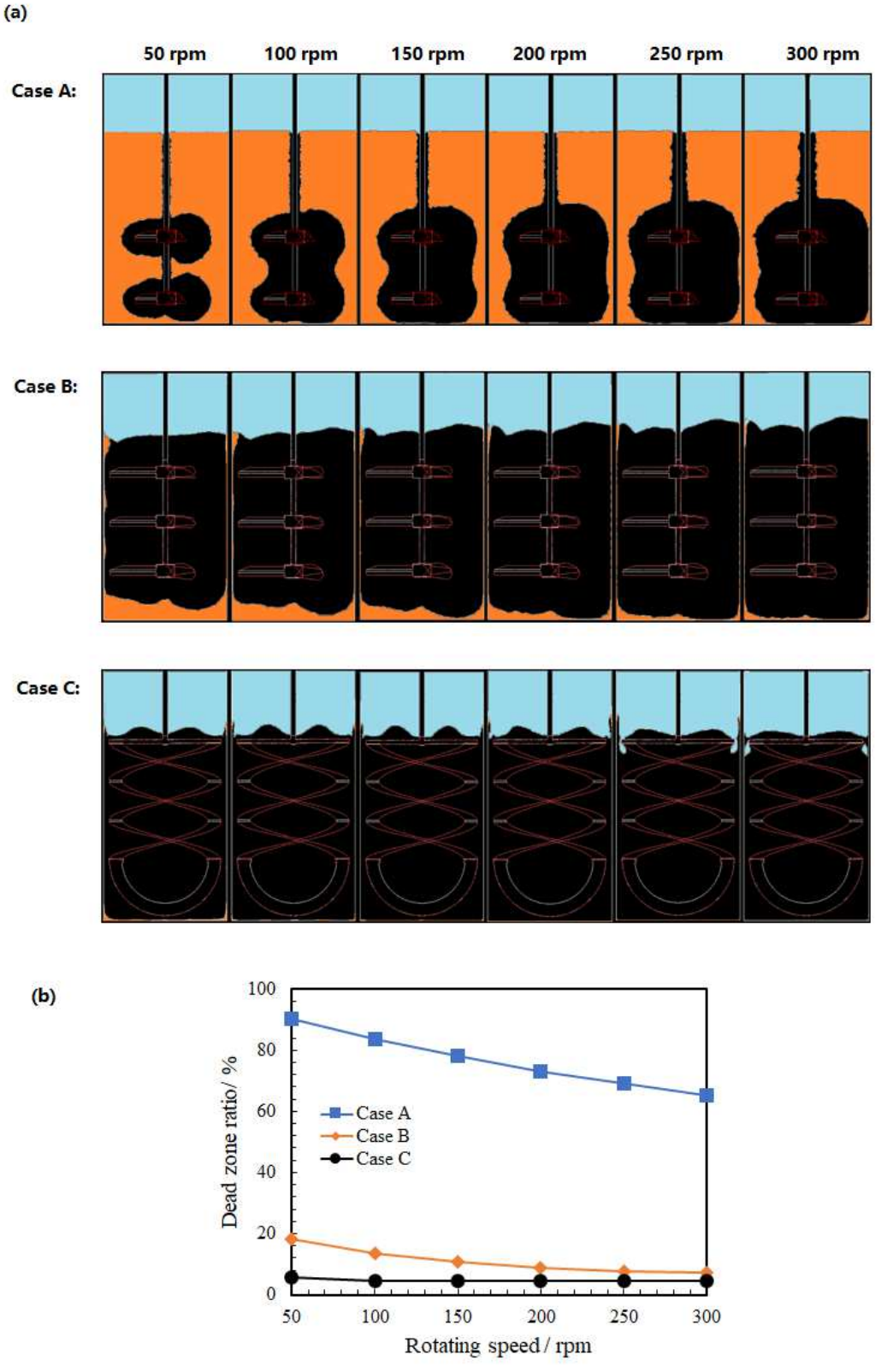

Fig.2 (a) Dead zone distribution in each cases at different rotating speed (the yellow section was the dead zone) and (b) dead zone ratio in each cases

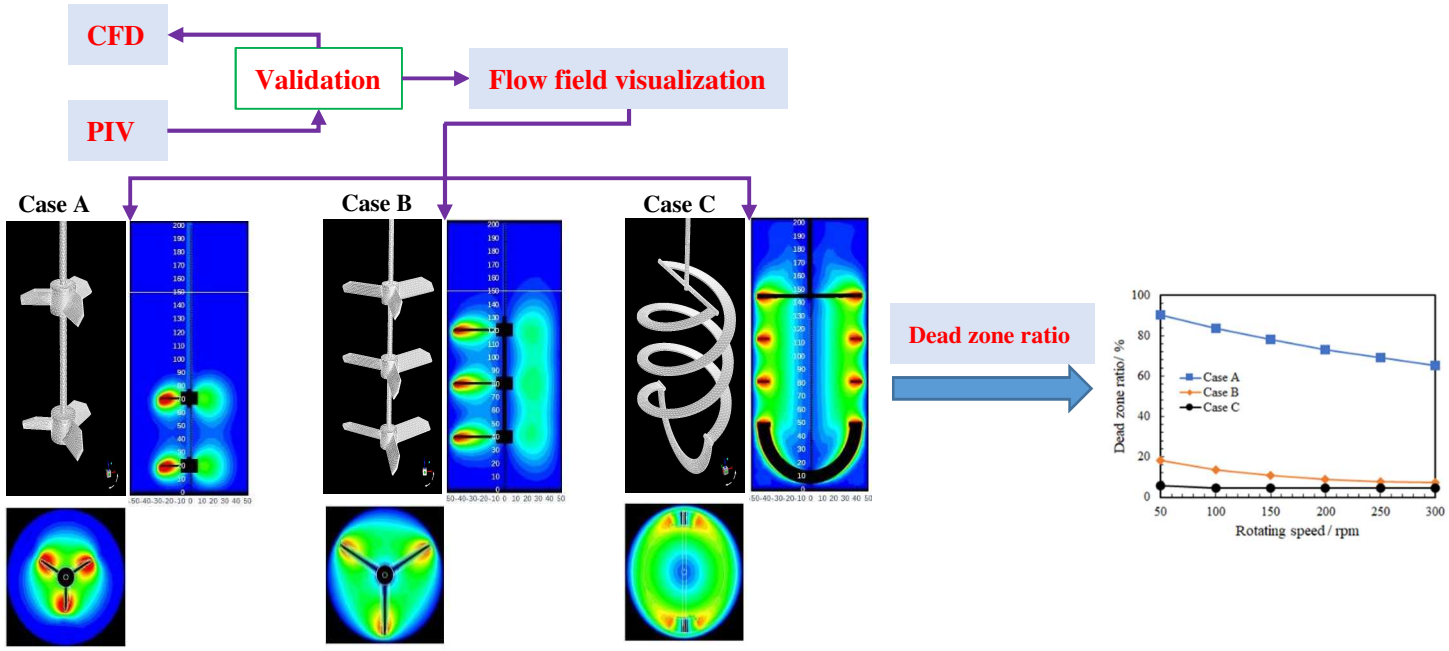
CFD
PIV
Validation
Flow field visualization
Case A
Case B
Case C
Dead zone ratio
Dead zone ratio/ %
Rotating speed / rpm
Case A
Case B
Case C